



Green 3D-printed lattice-shaped suspension arms for RC cars

Mohammadreza Lalegani Dezaki¹ · Mahdi Bodaghi¹ · Ahmad Serjouei¹ · Ali Zolfagharian²

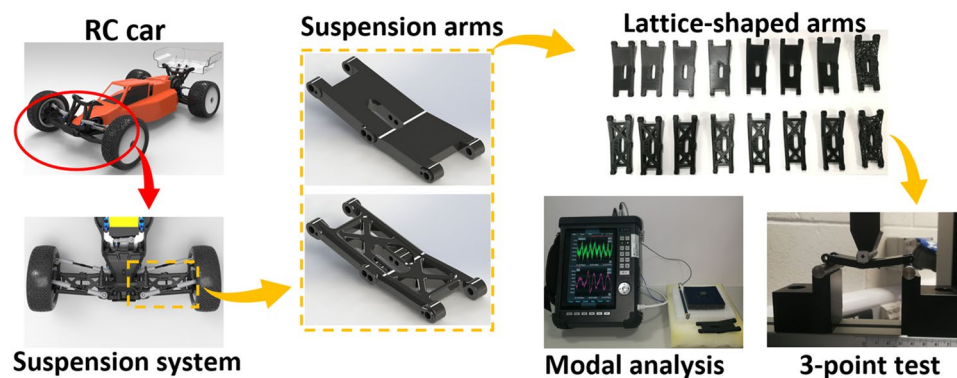
Received: 24 October 2022 / Accepted: 25 March 2023

© The Author(s), under exclusive licence to Springer Nature Switzerland AG 2023

Abstract

This study offers benchmark recommendations for designing lattice-shaped plastic suspension arms for remote-controlled (RC) automobiles in an environmentally sustainable manner. The main goals of sustainable and green design are to reduce the use of materials, minimise waste, and achieve a high-performance suspension system. A McPherson front suspension arm is designed with solid and optimised shapes and fabricated by fused deposition modelling (FDM) 3D printing. Solid, re-entrant honeycomb, face-centred cubic, hexagonal honeycomb, hexagonal prism diamond, simple cubic, triangular honeycomb, and lattice from a volume mesh are implemented on suspension arms in RC cars to investigate the effects of structural geometries on flexural strength and frequency response. Finite element analysis and experiment procedure are conducted to examine the deformation in four modes frequency shapes and critical areas in the suspension arms. The obtained results illustrate the relationships between the mass or stiffness and the vibration frequency.

Graphical abstract



Keywords Suspension system · Sustainable design · Lattice structure · Modal analysis · 3D printing · Fused deposition modelling

1 Introduction

Remote-controlled (RC) cars have been widely used in the past few decades. RC cars are commonly made of plastics and composites. One of the important elements in RC cars for driving performance is the suspension system, which is vital in the automotive industry. It consists of links, springs, shock absorbers, suspension arms, beam angles, and knuckles [1]. Different types of suspension arms have been developed for passenger safety and smooth handling. Double wishbone, short/long arm, and Macpherson strut

✉ Mahdi Bodaghi
mahdi.bodaghi@ntu.ac.uk

¹ Department of Engineering, School of Science and Technology, Nottingham Trent University, Nottingham NG11 8NS, UK

² School of Engineering, Deakin University, Geelong, VIC 3216, Australia

systems are independent systems that offer better handling and riding quality compared to a dependent system [2]. The Macpherson suspension has a lighter weight compared to the double-wishbone system. It is like the double-wishbone system, except that the upper arm is replaced with a long member called the “strut” [3].

Commonly, suspension arms are made from plastic or polymer-based composites in RC cars due to their lightweight, high performance, design flexibility, durability, and low cost [4]. Suspension arms are connected to the chassis and wheels to reduce vibrations and road noise [5]. Lower suspension arms handle the motion of wheels during driving. Also, a shock absorber and coil spring are attached to the suspension arm to increase the performance and durability of the chassis. The key role of suspensions is to isolate the chassis from forces and vibrations to have smooth driving with a lighter car. There are many ways to build plastic suspension arms. The common methods for producing RC vehicle components include injection moulding, casting, and additive manufacturing.

RC car components can fail in a variety of ways, but most of them are caused by stress, which can be triggered by unexpected road incidents. Also, components’ life service decreases due to the load history and environmental factors such as corrosion [6]. Design optimisation and choosing the proper material in the early manufacturing stage are the ways to avoid or eliminate these problems in suspension arms. Assigning a proper material leads to better performance and lighter weight in suspension arms, hence increasing fuel efficiency [7]. Reducing weight without sacrificing mechanical properties is the main goal of design and development. Designing complex products with lower weight leads to decreasing fuel consumption in RC cars. Reducing the suspension system’s weight without sacrificing mechanical strength increases the performance of RC cars in terms of fuel consumption and controllability. The sustainable and green design allows designers to modify and optimise the design accordingly. Implementing lattice shapes within the structure is one of the options which help to reduce weight.

Following that, computer modelling using finite element analysis (FEA) may be utilised to determine the behaviour of components under stress and how all physical stresses affect the design [8, 9]. Topology optimization and lattice structures can be employed to improve mechanical properties and reduce the weight of the products [10, 11]. Lattice structures have been widely used for their reliability and mechanical properties. Due to its design flexibility and dependability, three-dimensional (3D) printing is a trustworthy method for constructing lattice and complicated structures. Thus, 3D printing of RC components as a prototype or end-user product is another alternative way to produce plastic parts [12, 13].

Many approaches have been exploited to optimise vehicle components and improve suspension structure [14]. Öhammar et al. [15] made an RC car with polylactic acid (PLA) parts with the help of 3D printing technology. The printed RC car was analysed, and different suspension systems were assigned to record the performance. It was found that 3D-printed plastic products were able to work properly. Griese et al. [16] used the lazy part indicator method to find out potential areas for weight reduction in RC cars. Topology optimization was used to analyse and reduce the weight of components by changing their design. Finally, the weight of components could be reduced by 5% without sacrificing strength. Al-Asady et al. [17] examined and assessed the lower suspension arm to achieve acceptable accuracy by using crack initiation analysis. Maximum damage was found in the ball joint area. Furthermore, the majority of fatigue damage was recorded due to a large number of low-range cycles.

Kannan et al. [18] studied the printing parameters such as infill density, layer thickness, and extruder temperature to find out their effects on the natural frequency of acrylonitrile butadiene styrene (ABS), polycarbonate (PC), and ABS-PC materials. It was found that when the beams were clamped, the natural frequency was higher than clamped-free. Dunaj et al. [19] developed 3D-printed PLA covers with various thicknesses for a thin-walled steel beam to analyse its natural frequency. It was found that the PLA covers reduced amplitude by 37% of the first resonance function in the steel beam. Parpala et al. [20] found out infill density had the most effect on natural frequency by generating FEA and experimental methods. Results indicated increasing the wall thickness for the same mass, the natural frequency was decreased subsequently.

In spite of research work on suspension arms, there have been no studies on the vibration and strength of plastic suspension arms with lattice structural designs to have green and sustainable designs. The purpose of this research is to design and implement lattice structures to reduce the weight of suspension arms for RC cars without sacrificing strength. The aim is to increase driving performance by reducing the weight and increasing the strength of RC car components. The basic objectives of sustainability and green design are to reduce the consumption of materials, minimize waste, and create a high-performance suspension system. Modal analysis is used to find out the frequency response of the McPherson strut arm in different modes. Different lattice structures are implemented on two types of solid and optimised suspension arms in RC cars. After exploring the specimens’ properties in an FEA stage, solid and optimised samples are 3D-printed by the fused deposition modelling (FDM) process for dynamic and mechanical testing. FDM is used due to its availability in the market and low cost. Vibration analysis with the help of a dynamic mechanical

analyser (DMA) is carried out to examine dynamic behaviours. Finally, a comparison study is performed between each design to investigate their performances.

In the following sections, this paper is organized as follows: In Sect. 2, the lattice design and the procedure of 3D printing are discussed. In addition, methods for modal analysis and flexural strength of 3D-printed samples are explained. Details of results and discussion are provided in Sect. 3. Finally, Sect. 4 presents the conclusions and recommendations for future research.

2 Materials and methods

2.1 3D design and lattice shapes

The suspension load is carried by a suspension arm and sent to the spring or shock absorber. Suspension arms are typically used as part of the independent front suspension with MacPherson struts. Thus, it is vital to design suspension arms to have high strength and stiffness. In this research, the lower front arm of RC10B5M (Associated Electrics, California, USA) is used for analysis. The suspension arm used in this RC car is already optimised (original shape) by the company supplier and is available in the market as shown in Fig. 1(a).

This suspension arm is evaluated to have a better understanding in terms of strength and damping vibration. A solid design shape is outlined from the optimised version to investigate the effects of lattice shapes on strength and frequency response (see Fig. 1(b)). The optimised arm is changed to a rigid solid shape without fillets and chamfers accordingly. The 3D design of the optimised shape suspension arm with the details and sizes are shown in Fig. 1(c) and (d). Solid and optimised suspension arms are designed in SolidWorks software (version 2021, Dassault Systèmes, Vélizy-Villacoublay, France). The features such as curves and fillets are removed from the optimised shape to investigate the lattice designs on solid shapes. Both samples are evaluated through simulation and experiments. To ensure the accuracy of the results, the real-size sample is designed for both solid and optimised shapes.

To complete the procedure for the lattice design of the suspension arms, nTopology software (version 3.20, nTopology, USA) is used. The software enables you to apply a field-driven design approach and gives high accuracy and freedom in making various lattice structures. A cellular shape with a regular repeating pattern is known as a lattice structure [21–23]. Lattice structures can be used in different applications due to their deformability and properties in energy absorption [24–26]. Each design is modified by changing the thickness to show the differences in final 3D-printed

specimens because the mechanical behaviour of cellular structures is affected by structural topologies [27, 28].

Hence, two suspension arms are chosen to implement the lattice structure. The wall thickness of 2 mm is assigned to the suspension arms' shell. The minimum thickness of lattice structures must be 2 mm and values less than 2 mm result in failure in the printing procedure. This 2 mm thickness for re-entrant honeycomb, hexagonal honeycomb and triangular honeycomb is the wall thickness of repeated unit cells. Inside of these arms is filled with 2D lattice designs because of the small available area. If the 3D shape is implemented, the gaps inside the suspension arms are filled and bonding would be difficult due to the small size of lattice cells. Furthermore, seven different lattice shapes are chosen for both arms to investigate their influences on mechanical properties and frequency response. These types of lattices are chosen due to their reliable mechanical properties and usage of them in different applications. Other types of designs except these in this study need support structures inside the suspension arms and the results are changed drastically. The details and sizes of lattice types are constant as shown in Table 1. It should be noted, incomplete lattice cells or overlapping occurs in the design procedure. In fact, due to the real size of the suspension arms, changing the cell sizes will result in overlapping or incomplete unit cells again.

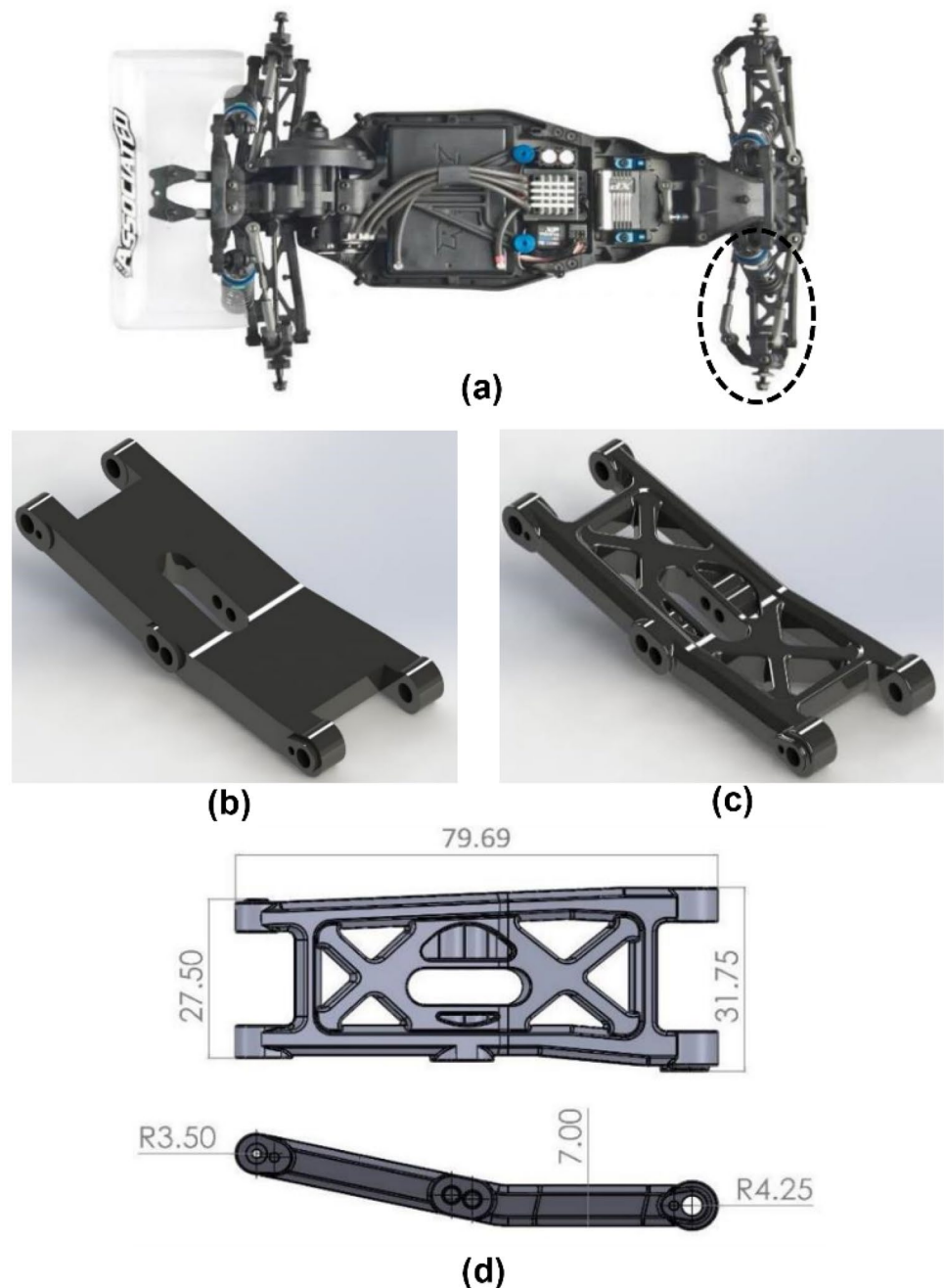
The values are constant for all samples to achieve accurate results. Table 2 provides the details of each lattice structure within the specimens. Different lattice designs are assigned to the suspension arms to investigate their effects on mechanical properties and modal analysis. The cellular structure of samples S8 and O8 is driven by a volume triangle mesh in nTopology software. The volume of the S8 and O8 suspension arms is like other arms without changing the details in the design. Thus, the volume mesh is assigned within the structure. The complexity of these two specimens is high while their weights are the lowest. The wall thickness of specimens is 2 mm to allow the 3D printer to fabricate them properly.

2.2 3D printing process

The printing procedure is carried out with the help of the FDM process. FDM is capable of printing complex lattice structures based on requirements from polymer to metal products [29–32]. Also, it is possible to use this technique to produce end-user products at a low cost which cannot be conducted by other 3D printing technologies. Products are 3D-printed from the bottom to the top with generated paths by software [33].

There are various printing parameters which affect the quality of finished 3D-printed samples. For example, build orientation, nozzle/bed temperature, infill pattern/density, layer thickness, and material flow rate are the main ones

Fig. 1 **a** Schematic of RC car structure. **b** 3D schematic design of solid suspension arm. **c** 3D design of optimised shaped suspension arm. **d** Details and sizes of the suspension arm



that have an influence on mechanical properties. In this case, Ultimaker Cura software (4.13 version, Ultimaker, Geldermalsen, Netherlands) is used to generate G-code which is readable by the 3D printer. The Ultimaker S3 machine (Ultimaker, Geldermalsen, Netherlands) is used to print all specimens. This machine has a dual extruder with a 0.4 mm nozzle diameter which results in a high resolution. PLA filament material from Ultimaker company (Ultimaker, Geldermalsen, Netherlands) is used, and the diameter of the filament is 2.85 mm. This biocompatible non-toxic material is durable with good adaptability and

simplicity in 3D printing procedures [34–36]. Also, it is available in different colours at a low cost in the market. All specimens are printed with the same parameters as shown in Table 3. Support for the base is used to avoid material drops during the procedure. No support is used inside the structure accordingly. The best build orientation with less support structure is 0° for all suspension arms. Other build angles result in more support structures and poor surface quality. Since the surface quality is not the main goal of this study, the layer thickness is set to 0.15 mm. Also, due to the low wall and cell thickness,

Table 1 Details of lattice parameters in nTopology

Sample no	Parameter	Value	Sample no	Parameter	Value
S1_O1	Blend type	Rounded	S8_O8	Edge length (mm)	100
S2_O2	Blend radius (mm)	0		Shape	Triangle
S3_O3	Shell thickness (mm)	2		Span angle (°)	30
S4_O4	Shell direction	Inward		Growth rate	2
S5_O5	Lattice cell scale X (mm)	5		Feature angle (°)	45
S6_O6	Lattice cell scale Y (mm)	5		Min edge length (mm)	0
S7_O7	Lattice cell scale Z (mm)	5		Thickness (mm)	2
	Fill type	All touching	–	–	–
	Lattice cell thickness (mm)	2	–	–	–
	Beam thickness (mm)	2	–	–	–

100% infill density is assigned to avoid material drop and poor printing.

Printing S8 and O8 specimens are different from the other arms. Due to the high complexity of these two samples, the machine is not able to print them directly. Thus, another support material was used to complete the task. White poly-vinyl alcohol (PVA) filament from Ultimaker is used as a support material. This biodegradable material is a water-soluble support material for multi-extrusion 3D printing. It is compatible with a 0.4 mm BB print core (Ultimaker, Geldermalsen, Netherlands) which is for support materials and the diameter of the filament was 2.85 mm. The parameters of the second nozzle are shown in Table 3. After printing was finished, these two specimens are put into the water for 3 h to remove support materials. All 3D-printed samples are shown in Fig. 2. Their weights are equal to the design one as shown in Table 2.

2.3 Experimental modal analysis

Vibrations affect car components due to the interaction between the tyres and the road. These vibrations affect the mechanical properties and life cycle of plastic components [37]. Thus, the material and design are critical to reducing vibrations and increasing efficiency. A method to extract natural frequencies, damping, and mode shapes with the use of the time or frequency domain is known as a modal analysis [38]. Frequency response functions (FRFs) are used to find resonant frequencies. The procedure can be done through an impact hammer test with the assistance of a DMA. This method allows one to analyse suspension arms to find out their natural frequency and various modes [39].

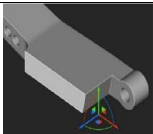
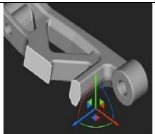
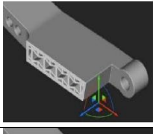
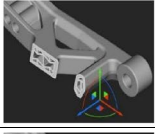
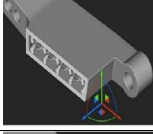

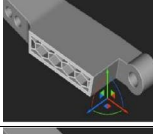
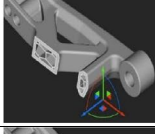
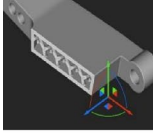
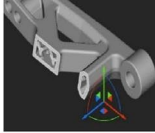
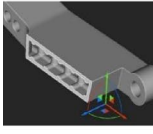
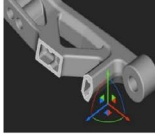
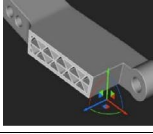
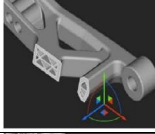
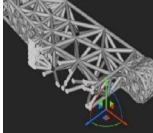
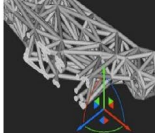
The experimental modal analysis in this study is performed with the dynamic signal analyser (DSA) CoCo-80X from Crystal Instruments (Santa Clara, California, USA). The frequency responsiveness of the structure may be estimated by measuring both the input and the response. Calculating the frequency response at numerous points, either simultaneously or separately, will provide data that may be

used to estimate the structure's dynamic reaction. Measuring the responses is done with the impact hammer modal test. TLD356A16 triaxial ICP® accelerometer from PCB Piezotronics with 100 mV/g sensitivity and 0.3 to 6000 Hz frequency range is assigned for hammer test. Also, 086E80 ICP® impact hammer with 22.5 mV/N sensitivity and 222 N pk measurement range was used to conduct results as shown in Fig. 3(a). A piece of foam is used to eliminate damping and vibration from external stimuli during the procedure.

One side of the samples is pinned clamped since the suspension arms in RC cars are pinned to the tyre, chassis, and shock absorber. A 3D-printed structure is used to hold the suspension arm accordingly. This area is chosen for the impact hammer test. The accelerometer is placed under the sample covered by foam on the other side. The side that the accelerometer is assigned is placed on the foam to eliminate additional vibration. The schematic of the procedure is shown in Fig. 3(b). Typically, foam is selected to create the free boundary conditions possible for modal analysis, while still enabling the operator to conduct the test. As such, the foam serves to balance out the static behaviour of the component without affecting its dynamic behaviour. However, it should be noted that the foam can only compensate for the static weight of the accelerometer at best, and the addition of an appreciable amount of mass to the component will still alter its dynamic response. It means the attached accelerometer affects the results of the modal analysis.

After collecting data and achieving results within the CoCo-80X, generated data are transformed into the software. Engineering data management (EDM) software (version 2021, Crystal Instruments, California, USA) is used to analyse and edit data. The first four vibration modes are considered with normalized FRF value. The settings in CoCo-80X are 1.88 kHz frequency range, 1024/450 block size, 10 Hz frequency resolution, and linear averaging with an average of two hits at the same point. The linear average mode applies to the frequency domain, power spectra averaging. Time linear applies to time domain averaging.

Table 2 Design of lattice structures for solid and optimised suspension arms

Lattice	No. (Weight) (gr)	Solid shape	No. (Weight) (gr)	Optimised shape
Solid	S1 (12.67)		O1 (11.64)	
Re-entrant honeycomb	S2 (9.67)		O2 (7.70)	
Face centred cubic	S3 (8.36)		O3 (8.16)	
Hexagonal honeycomb	S4 (7.76)		O4 (7.61)	
Hex prism diamond	S5 (9.86)		O5 (8.71)	
Simple Cubic	S6 (7.89)		O6 (7.34)	
Triangular honeycomb	S7 (7.96)		O7 (7.33)	
Cellular structure	S8 (6.37)		O8 (5.83)	

Damping and natural frequency of different modes are calculated to investigate the effects of lattice structures on properties.

2.4 Flexural test

In this study, flexural testing with a 3-point bending test is conducted to determine the characteristic strength of the components. To investigate their strength, the test procedure for suspension arms is conducted for each sample. Shimadzu AG-X plus machine (Shimadzu, Shimadzu UK, UK) is used and TRViewX (Shimadzu, Shimadzu UK, UK) recorded the

data accordingly. Figure 4(a) and (b) illustrate the arrangements for the 3-point bending test of 3D-printed arms. Both sides of the samples are clamped using double-sided tape to avoid any movements during the test. A force rate is applied, and the deflection is recorded until the failure happens. Meanwhile, the deflection is recorded continuously. The crosshead speed is set to 1 mm/min due to the samples' size. A set of three samples are used for the 3-point bending test. Also, the force is applied to the area where the shock absorber is connected. Since the load is not along the machine axis, the orientation is considered in TRViewX software. The flexural test and modal analysis are conducted

Table 3 3D printing parameters and materials

Parameters	PLA (Main material)	PVA (Support material)
Sample	All samples	S8 & O8
Build angle	Flat (0°)	Flat (0°)
Nozzle diameter (mm)	0.4	0.4 BB type
Layer thickness (mm)	0.15	0.15
Infill pattern	Linear	Linear
Infill density (%)	100	20
Nozzle temp. (°C)	210	225
Bed temp. (°C)	60	60

to investigate the suspension arms in terms of maximum force and frequency mode.

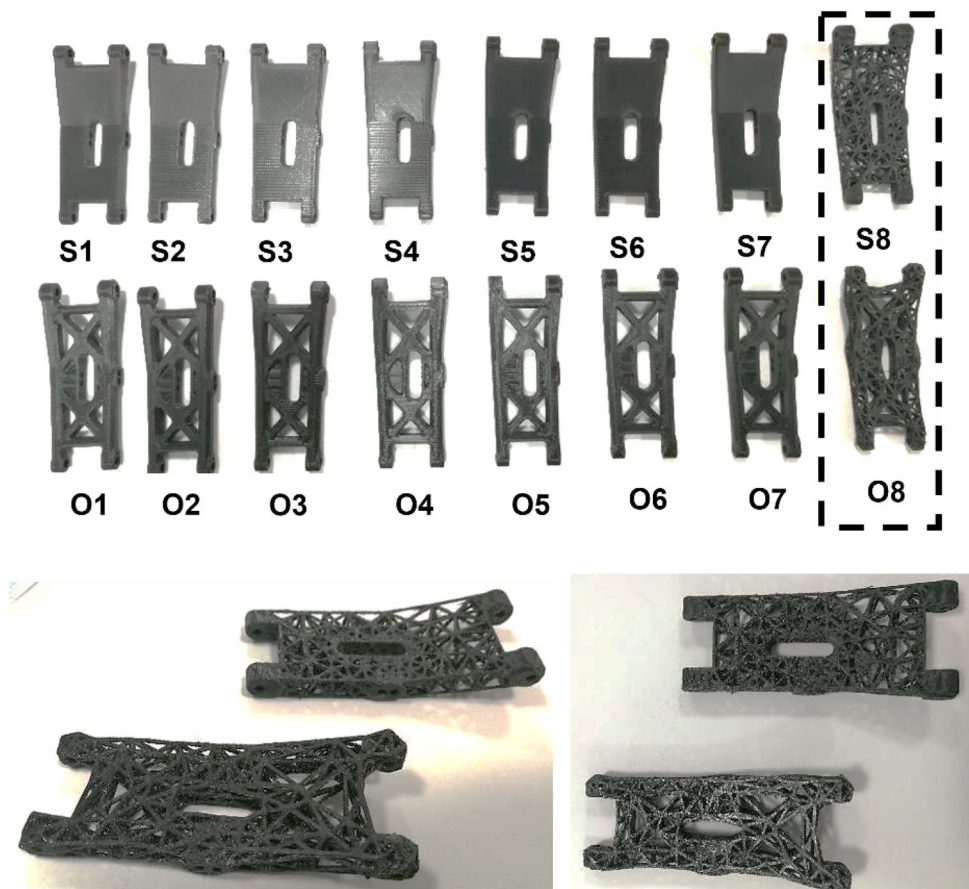
2.5 Finite element analysis

The simulation procedure is done through Ansys software package (version 2021, Ansys, Inc., Pennsylvania, USA). Modal analysis is performed to evaluate the mode shapes and structural static is done to investigate the critical area in the elastic phase. In modal analysis, one side of the arms is

pinned which allows the structure to rotate in one direction same as the experimental procedure. The other side of the suspension arm is free since it is placed on the foam in the experimental procedure. The weight of the accelerometer is considered in simulation as a point mass of 70% of the arm's weight since it is under the suspension arm affects the results. The point mass is placed below the structure as followed in the experiment. Tetrahedral mesh mode with the size of 3 mm is assigned to both samples and a convergence study by reducing mesh size to 2 mm and 1 mm locally and run time is performed to ensure the results are accurate. PLA material is assigned for both procedures. The material properties of PLA samples are obtained according to ISO 527 standard tensile test on three 3D-printed dog-bone samples [40]. Dog-bone specimens are printed in 0° build orientation and the printing patterns and lines are aligned with the tensile direction.

The density of the dog-bone PLA sample is 1250 kg/m³ and mechanical properties are given by Ansys with average values of 2.62 GPa Young's modulus, 44.70 MPa ultimate tensile stress (UTS), and 0.14 break strain. Adding the obtained results of the tensile test, the behaviour of the material in the plastic region is investigated as well. The material is nonlinear isotropic in this case and the displacement load

Fig. 2 3D-printed lattice suspension arms



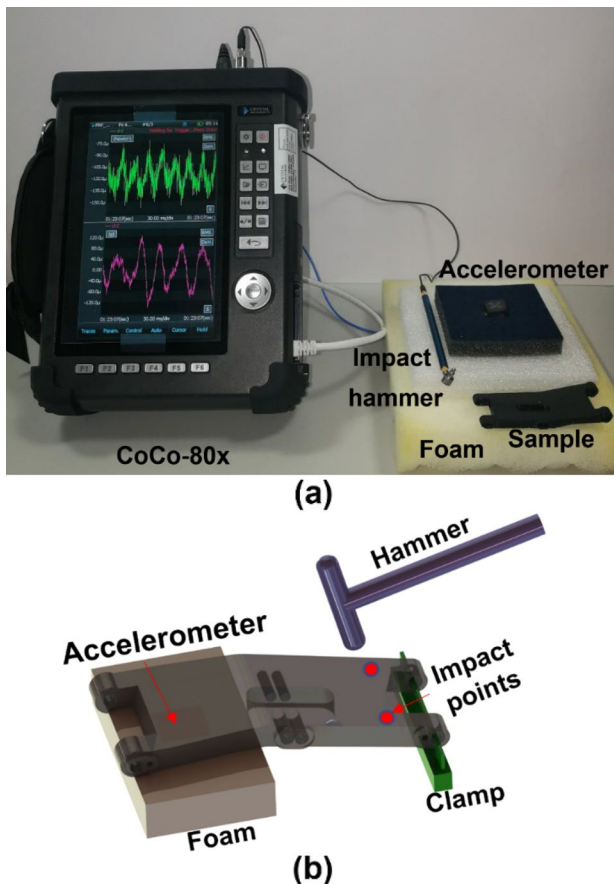


Fig. 3 **a** Components for modal analysis and **b** 3D schematic of the modal analysis procedure

is applied. In order to account for geometric nonlinearity in that step, the option NLgeom is considered. The data of the stress–strain curve is imported to Ansys and the multilinear isotropic hardening approach is used to show the elastic and plastic regions under a constant load. The mechanical test is done by the Shimadzu AG–X plus (Shimadzu, Shimadzu UK, UK) with a speed of 0.30 mm min^{-1} . The average result

of the tensile tests of 3 dog-bone samples is shown in Fig. 5. Modal analysis is done in the range of 0 Hz to 1500 Hz to find out the mode shapes of samples for the first four modes. Meanwhile, the structural analysis is conducted to investigate the deflection and cracked point in 3-point bending tests. The same boundary condition in the experiment with only one degree of freedom constrained is followed in simulation and a displacement rate is applied in the middle of the arms where the shock absorber is connected.

The only way to export the design from nTopology software is by converting solid lattice into mesh design for further analysis. Lattice designs in the nTopology software are exported in the form of tetrahedral mesh with size of 3 mm and with 16,216 elements. The mesh design is imported to Ansys software, and no further modification can be done on the meshes. Total deformation for structural analysis and deformations in the first four modes are recorded.

3 Results and discussions

Suspension arms with various lattice structure cores arrangements are investigated in this study. By running flexural strength and modal analysis tests on those combinations, it is possible to find out the optimum design among them. Higher strength in plastic suspension arms leads to better performance in terms of shock absorption in RC cars. However, strength is not the only factor in driving conditions. It is crucial to minimize the weight of the suspension system since the weight of the RC car is so substantial. Typically, structural designers aim to enhance the structural performance by optimizing either the size or topology, or to reduce the structural weight as much as possible. In this study, suspension arms with optimised shapes have lower weight compared to solid shape arms. This implies that through the optimized shape design, the weight can be reduced without compromising the strength of the suspension arm. The objective is

Fig. 4 3-point bending tests in **a** schematic shape and **b** experimental test

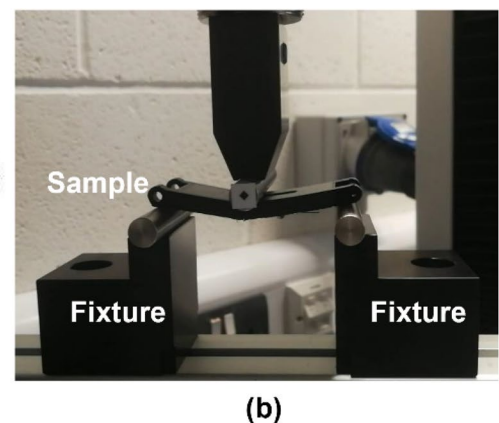
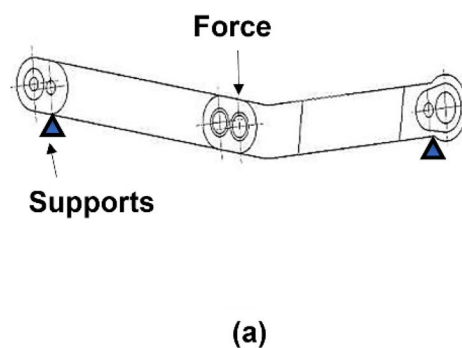
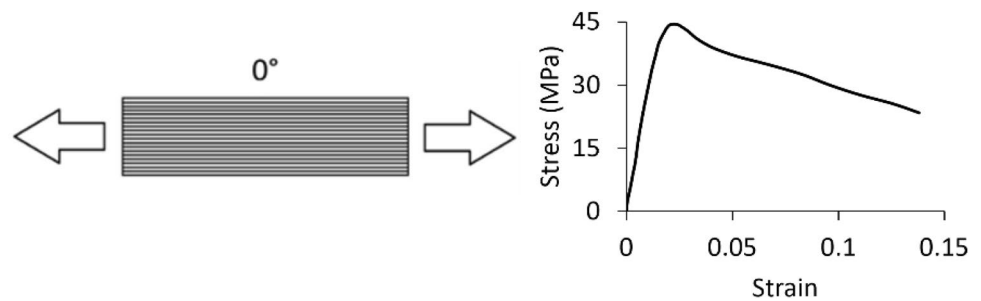


Fig. 5 The average result of tensile stress–strain curves of PLA material



to improve the efficiency of RC cars, lower energy usage, and decrease the amount of material waste.

Additionally, mechanical damping forms the core of modern suspension. The modal analysis conducted in this study provides crucial information for understanding the dynamic behaviour of suspension arms. The damping ratio is a crucial factor to consider when designing a suspension system as it affects the suppression of spring oscillations. However, beyond a certain point, the damping ratio has a limited impact. Generally, high damping ratios result in little change in the resonance frequency. The damping ratio varies depending on the intended use of the vehicle. The driving performance is better when the damping ratio is higher. Meanwhile, better comfort is achieved when the damping ratio is lower. However, this is typically true when adjusting damping around a default value, although it might not be accurate in absolute terms because comfort can still be negatively impacted by very low or zero damping.

The results of FRF sections are provided to investigate the details of the damping factor and natural frequencies in the first four modes which allows one to find out the effects of PLA properties and structure design in dynamic analysis. A common method that is used in modal analysis to compute several repetitions is the averaging of the power spectrum. Proportional integral derivative (PID) tuning frequently employs power spectrum analysis, which uses a fast Fourier transform (FFT) to calculate the frequency spectrum of a certain signal from its fluctuation. The figures of force magnitude, acceleration, frequency response, and coherence for sample S1 were generated using MATLAB® (version 2021, MathWorks, Massachusetts, USA) and shown in Fig. 6.

Coherence is the property of a linear system in which a frequency input generates an output signal. The shock or impact test modules provide an analyser graph option called coherence. The value of the periodogram for FRF is less than 1 kHz with an 11 N impact force. FRF and FFT are obtained directly through a data acquisition system. The force and acceleration of the impact hammer procedure are shown in Fig. 6(a) and (b). As shown in Fig. 6(c), amplitude and phase are transformed into real terms. The natural frequency and damping of each mode are derived from the FRF

graph. Normally, the range of frequency for all samples is between 0 and 1 kHz. A closer look reveals a strong peak of up to 50 dB at 780 Hz. To avoid noise realization during the frequency response, the resolution is limited to 1.88 kHz. Also, the coherence shows the quality and consistency of the FRF.

Figure 6(d) displays the coherence of the frequency response of the sample S1 in different modes. Results indicate that when the amplitude of FRF is high, the value of coherence is close to 1 at the resonant frequency. At anti-resonance, which is 280 Hz, the coherence value is close to 0. It is noted that low coherence around anti-resonance frequencies is evident in the results, which is a standard behaviour in this case. Meanwhile, if the value of coherence is close to 0 instead of 1 across the entire frequency range, the procedure is followed with a leakage between each 3D-printed layer [41]. This means due to the layer-by-layer binding, there may be tiny gaps between each layer which affect the damping and resonance. The vibration is affected due to the non-contact regions between layers.

In this study, other specimens follow the same FRF behaviour while the natural frequencies in different modes varied due to the lattice structures inside the suspension arms. Hence, to make a comparable study, the main impacts of parameters are done by grouping suspension arms based on frequency in each mode. This means the average value of damping and frequency are recorded accordingly. The calculation of these factors is done in EDM software automatically. After analysing the results without any double impact and overload in the hammer test, the natural frequencies and the percentage of damping are shown in Fig. 7. The results are used to compute the modal of the structures at specific locations. Small changes in amplitude and peak value are observed in FRFs graphs.

As shown in Fig. 7(a) and Fig. 7(b), the value of the natural frequency of arms increases consistently in higher modes from 100 to 1000 Hz. Meanwhile, the percentage of damping decreases step by step from 3% to 0.7% in both designs as shown in Fig. 7(c) and Fig. 7(d). This means damping in higher frequencies becomes lower and the FRF graphs show tighter peaks and valleys. Also, the natural frequencies in

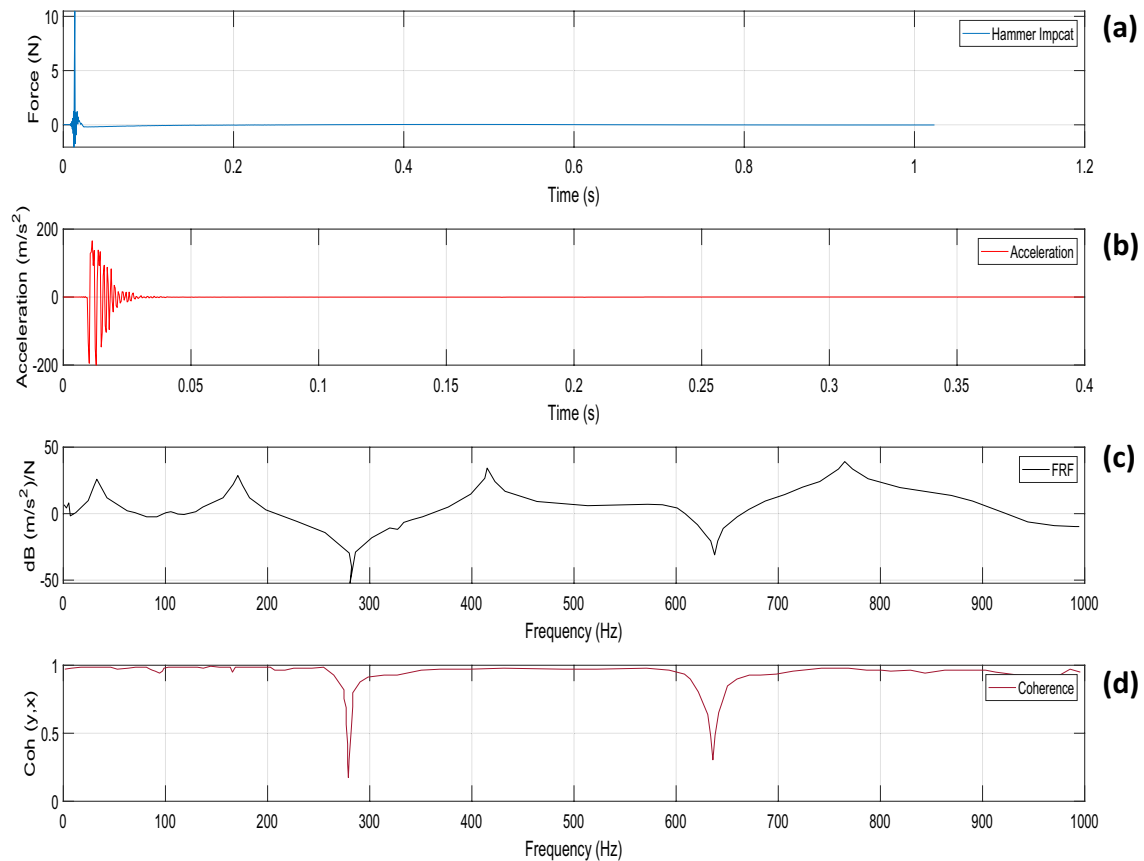


Fig. 6 The average results of **a** force, **b** acceleration, **c** FRF, and **d** coherence for the S1 specimen

the first four modes in optimised suspension arms are higher than in solid shapes, while the value of damping is the lowest. Based on the provided bar charts, sample O8 has the highest frequency except in mode 1, in which sample O3 has the highest frequency among specimens. The same thing happens to solid arms, and S8 sample shows a higher frequency in all 4 modes. However, the results in damping are not the same and showed different values. This is because of the presence of lattice structures within the suspension arms. It is found that the lattice structures play an important role in damping. In solid arms, the highest damping is for sample S4 in mode 1 while sample O3 has the highest damping among optimised arms. However, the damping is different in other modes due to the complexity of suspension structures. For example, damping in optimised samples is lower compared to solid ones. In addition, higher damping is recorded for samples O1 and O3 in mode 4 while S1, S3, and S4 damp more vibration.

The natural frequency of arms in both groups is almost equal due to the similarity in structure. Results show that there is a relationship between mass and frequencies. By increasing the mass, the frequency decreases while the weight of arms is dependent on lattice design and FDM

parameters. Despite these differences, the weight of optimised arms is lower than solid samples which leads to a higher frequency and lower damping in this study. Besides, four different mode shapes of solid and optimised arms are derived from Ansys Workbench (version 2021, Ansys, Inc., Pennsylvania, USA), as shown in Fig. 7(e) and (f). The first mode shows linear deflection follows by twisting and bending deflection. In all samples, the damping decreases from 3% to 0.7% by increasing the mode frequencies from 100 to 1000 Hz.

The mode shapes and natural frequencies provide information at which frequencies the system is vulnerable to vibration. The mode shapes of these two suspension arms show how to change the natural frequencies out of the range of excitation frequencies. In these two specimens, the regions that are attached to the tyre and shock absorber may experience high stresses if the deformed shape is like the mode shapes. The mode shapes of solid and optimized specimens are similar except for mode 2 due to the changes in shapes and design. The deformation that suspension arms exhibit while vibrating at their inherent frequency is described here. However, unless there is an excitation, neither vibration nor deformation takes place. Also, mode

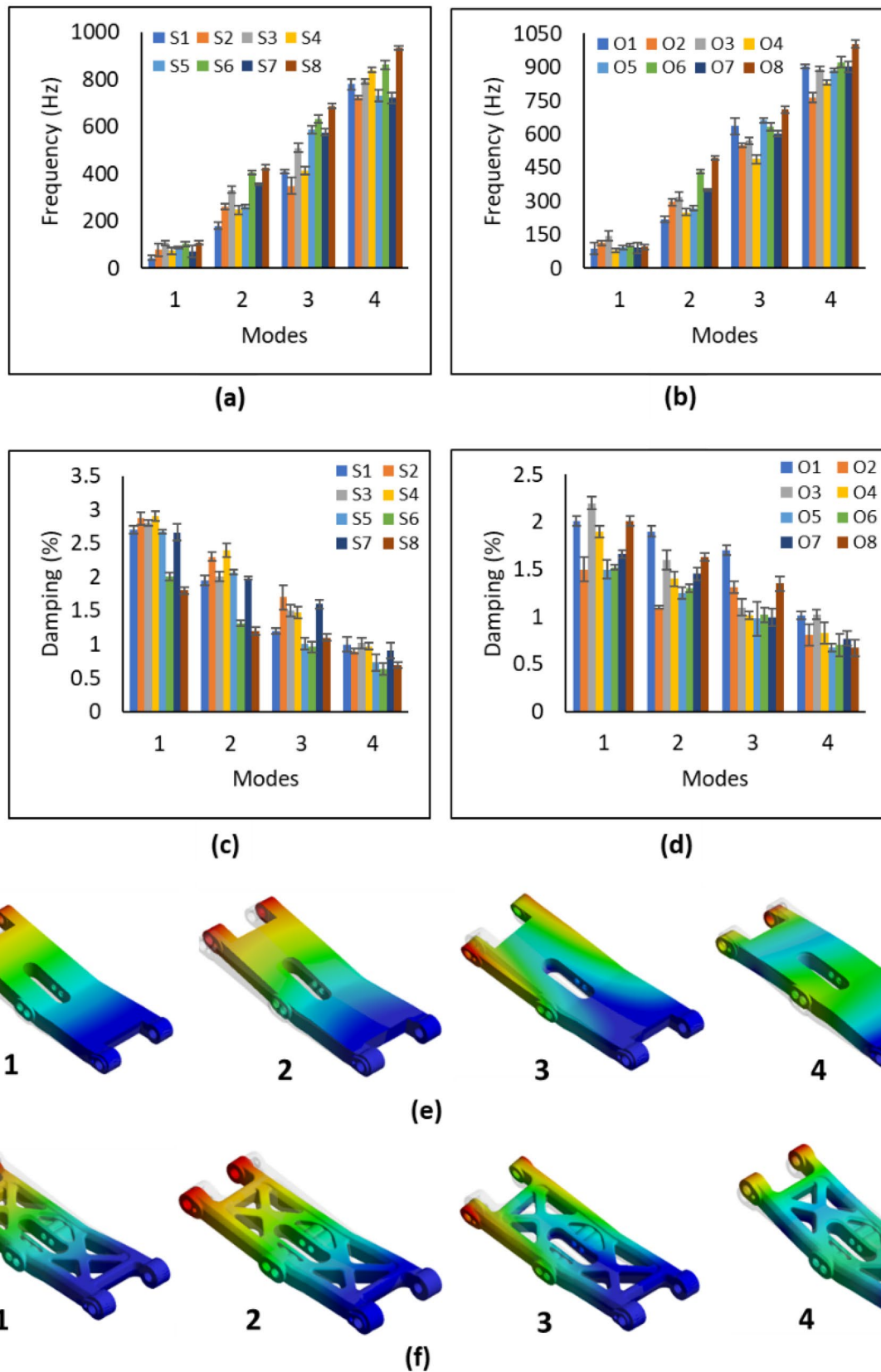
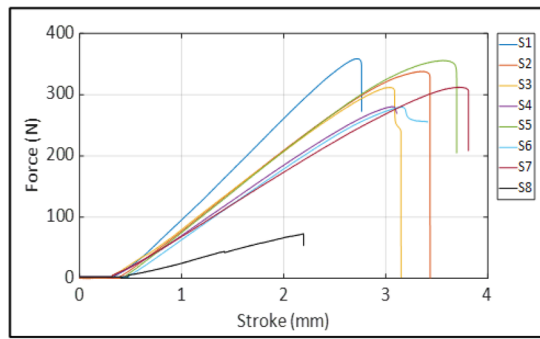
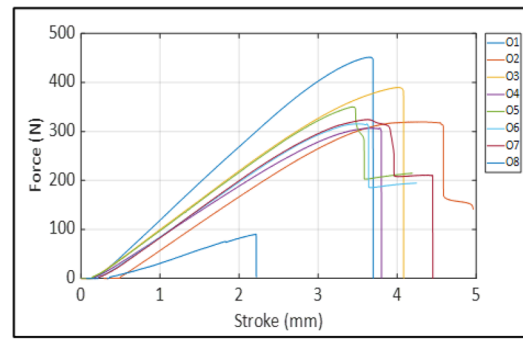


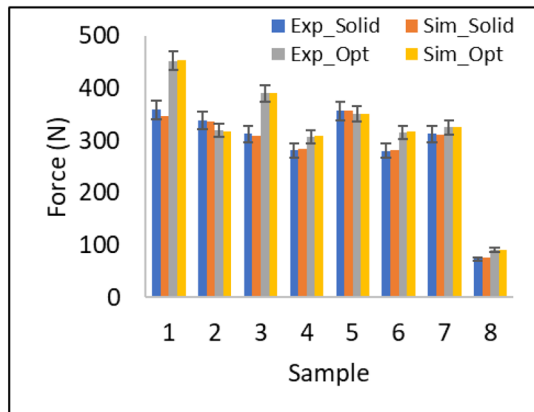
Fig. 7 Average mode frequencies of **a** solid and **b** optimised arms with damping percentages in **c** solid and **d** optimised arms. Overview mode shapes of **e** solid and **f** optimise suspension arms



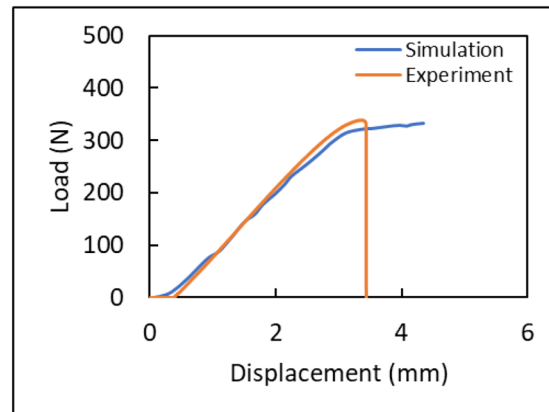
(a)



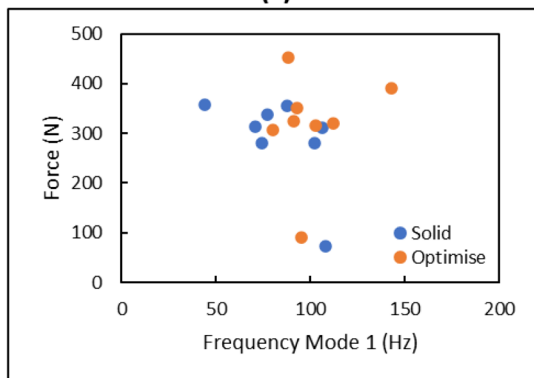
(b)



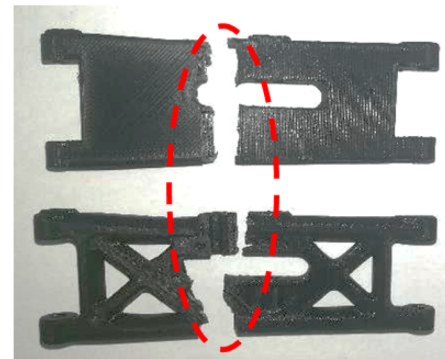
(c)



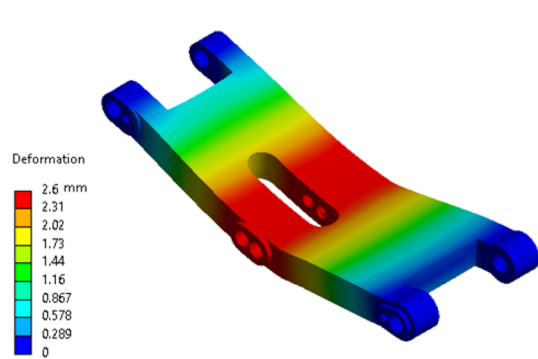
(d)



(e)



(f)



(g)

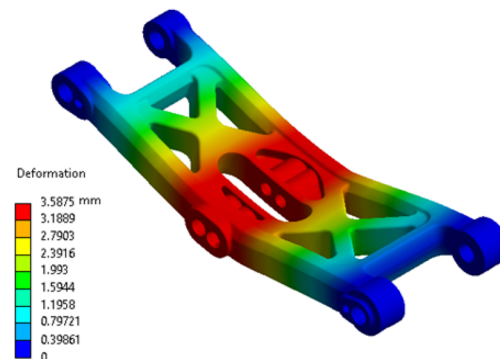


Fig. 8. 3-point bending experimental test results for **a** solid and **b** optimised suspension arms. **c** Experimental and simulation results of force within the same displacement range for solid and optimised samples. **d** The force–displacement graph of simulation and experiment for the S2 sample. **e** The force versus frequency mode 1 for samples S1 and O1. **f** Failure and cracked area in suspension arms. **g** Deformation of suspension arms in simulation procedure

shapes reveal the behaviour of the structure under a dynamic load.

Flexural testing studies on these objects additionally allowed researchers to examine how structural design affects the strength of specimens. Figure 8(a) and (b) show the force that is applied to samples. The applied force varies due to the different internal lattice structures. Figure 8(c) provides information about the maximum flexural strength of all suspension arms. The 3-point bending test is done on samples to show the differences accordingly. In terms of finding the load in simulation, a force–displacement graph from simulation and experiment is used. A node is set to measure the applied force when the displacement reaches the same value in the experiment. Increasing the load due to the nonlinear behaviour, the information of the load–displacement curve within the same displacement range can be derived as shown in Fig. 8(d). No damage model was implemented but the simulations were still quite accurate over the whole force–displacement curve range. The standard deviation shows the difference between maximum force in solid and optimised samples which are 2% and 3%, respectively. Also, the same results are obtained for frequency and damping. It is observed that topology optimization can improve mechanical properties. Optimised suspension arms tolerate more stresses compared to the solid specimens, except for samples O2 and O5. The toughest suspension arm is O1 with a value of 451.67 N force followed by the O3 sample which is the face-centred cubic sample and cracked at 390 N force. This order is followed by samples S1, S5, and O5 which have higher strength and are hexagonal prism diamond lattice shapes. The reasons that the optimised sample has higher peak stress are fillets and chamfers throughout the sample.

Fillets and chamfers distribute stresses in specific regions. Hence, the force is minimised in cracked areas. Therefore, the optimised samples especially sample O1 are stronger. Meanwhile, all the fillets and chambers are removed in solid shapes which leads to lower strength. The solid sample (sample S1) cracked faster than the optimised sample (sample O1). It should be noted that due to the lattice design inside the suspension arms and the internal contact between lattice structures and suspension shells, the results are different in other samples accordingly. The forces for the weakest samples are 73.07 N and 90.77 N for samples S8 and O8, respectively. However, printing parameters were also effective, which are constant in this study. Figure 8(e) shows the maximum force versus frequency in mode 1. It can be clearly

seen all samples' frequencies in mode 1 are between 70 and 150 Hz for both groups with different maximum forces. It shows the results are close to each other due to the similarities in based design.

Obtained data indicate that flexural strength varies in the same direction as the natural frequency of the first four modes. Also, damping is improved due to the ductility of thermoplastic PLA material. Additionally, the natural frequency and resonant frequency increase with an increase in flexural strength. Meanwhile, natural frequency affects mechanical properties in a dynamic system. However, clamping is also effective on obtained natural frequency. It is found that flexural strength has a direct link with the natural frequencies of lattice structures. As shown in Fig. 8(f), the flexural results show the critical area in all specimens. It is suggested to modify the pinned areas or make the holes thicker. This section is connected to the shock absorber which handles the driving task. The displacement is 3.58 mm for O1 and 2.6 mm for S1 which is conducted from the simulation procedure (see Fig. 8(g)). Also, the maximum force in simulation is close to the experimental data. For example, the maximum force in simulation for optimised samples is 453.42 N which is close to the experimental counterpart with the value of 451.67 N for sample O1. The same results are conducted for all 3D-printed samples. The strongest specimens in solid shape are S1 and S5, respectively. Also, O1 and O3 are the strongest suspension arms among optimised shape specimens.

In this study, driving performance has priority over comfort. Thus, higher damping is suitable for RC cars in this case. In mode 1, the face-centred cubic arm in optimised specimens has higher damping ratios which results in better driving performance. It has the highest damping ratio in mode 4 as well. Meanwhile, in solid shape suspension arms, hexagonal honeycomb has a higher damping ratio in mode 1. In mode 4, the face-centred cubic arm has the highest damping followed by the hexagonal honeycomb arm. Also, face-centred cubic arm shows higher strength in the specific areas while its weight is 8.16 g compared to the solid one which is 11.64 g. Hence, the face-centred cubic arm is a good alternative design which can be used instead of a solid optimised shape. On the other hand, hex prism diamond shows higher strength while its weight is 2.81 g lower than the solid specimen in solid shape arms.

In brief, face-centred cubic arms in optimised shape suspension arms show better performance in terms of strength and damping ratio in static analysis. This implies that employing this lattice design results in lighter RC vehicles without sacrificing driving performance. Using PLA as a material helps to have a green design and reduces material wastage by design optimisation which leads to design sustainability. It is recommended to analyse these designs and the whole suspension system in driving conditions

to evaluate their performance in dynamic situations. This design will increase driving performance and reduce power consumption to save energy.

4 Conclusion

In this study, 3D printing of sustainable and green lattice-shaped suspension arms of RC cars with high dynamic and mechanical performance was investigated. The proposed work was vital to pave the way to optimise and increase the efficiency of RC cars and mobile robots. The green design helps to decrease the weight and power consumption of RC cars. Solid, re-entrant honeycomb, face-centred cubic, hexagonal honeycomb, hex prism diamond, simple cubic, triangular honeycomb, and cellular lattices from volume mesh were studied in this work. Modal analysis and flexural tests were conducted to examine the strength and frequency of each lattice shape. The damping and natural frequency in the first four modes were recorded to understand the relationship between flexural strength and vibration amplitude. The findings are as follows:

- This work showed how to print complex structures and the advantages of optimization in increasing mechanical properties at specific regions.
- The method is used to reduce material wastage without sacrificing mechanical performance.
- The proposed technique is useful for sustainability and green design to reduce weight and enhance fuel efficiency.
- It was recorded that the mechanical properties were changed in different lattice structures.
- Natural frequencies had a direct relationship with mechanical properties, according to the experimental modal analysis of 3D-printed materials.
- The natural frequencies of the arms were between 50 Hz and 1 kHz found from investigating the first four modes.
- Results indicated that face-centred cubic in optimised samples and hex prism diamond were reliable in terms of strength and vibration damping after solid shape suspension arms.
- It was found that optimization and sustainable design reduced the structure weight, improved the specific strength at regions under load and affected vibration damping.
- Future research on this work can be done on the dynamic stability of mobile vehicles and the integration of the whole suspension system to examine the overall deflection and vibration in the real world.

Data availability The data that support the findings of this study are available from the corresponding author upon reasonable request.

Declarations

Conflict of interest The authors declare that they have no conflict of interest.

References

1. Kashem S, Nagarajah R, Ektesabi M (2018) Vehicle suspension system. In: Kashem S, Nagarajah R, Ektesabi M (eds) Vehicle suspension systems and electromagnetic dampers. Singapore, Springer Singapore, pp 23–37
2. Sun W, Gao H, Shi P (2020) Background, modelling and problem statements of active suspensions. In: Sun W, Gao H, Shi P (eds) Studies in systems decision and control. Springer International Publishing, Cham, pp 1–13
3. Gadola M, Chindamo D, Legnani G, Comini M (2019) Teaching automotive suspension design to engineering students: bridging the gap between CAD and CAE tools through an integrated approach. *Int J Mech Eng Educ* 47:23–43. <https://doi.org/10.1177/0306419018762803>
4. Pawi FT, Daud R, Ayu HM, et al (2019) Design and analysis of lightweight polyetheretherketone (PEEK) front lower control arm. In: AIP Conference Proceedings. p 020026
5. Kim YD, Jeong JE, Park JS et al (2013) Optimization of the lower arm of a vehicle suspension system for road noise reduction by sensitivity analysis. *Mech Mach Theory* 69:278–302. <https://doi.org/10.1016/j.mechmachtheory.2013.06.010>
6. Yıldız BS, Lekesiz H (2017) Fatigue-based structural optimisation of vehicle components. *Int J Veh Des* 73:54. <https://doi.org/10.1504/IJVD.2017.082579>
7. Park JH, Kim KJ, Lee JW, Yoon JK (2015) Light-weight design of automotive suspension link based on design of experiment. *Int J Automot Technol* 16:67–71. <https://doi.org/10.1007/s12239-015-0007-4>
8. Singh J (2015) Static structural analysis of suspension arm using finite element method. *Int J Res Eng Technol* 04:402–406. <https://doi.org/10.1562/ijret.2015.0407064>
9. Li Y (2021) Finite element structure analysis of automobile suspension control arm based on neural network control. *Secur Commun Netw* 2021:1–11. <https://doi.org/10.1155/2021/9978701>
10. Jawad BA, Polega BD (2002) Design of Formula SAE Suspension Components. In: SAE Technical Papers
11. Płaczek M, Ariffin MKA, Baharudin BHT, Lalegani Dezaki M (2021) The Effects of 3D printing structural modelling on compression properties for material jetting and FDM Process. In: Kyratsis P, Davim JP (eds) Experiments and simulations in advanced manufacturing. Springer International Publishing, Cham, pp 171–194. https://doi.org/10.1007/978-3-030-69472-2_7
12. Mohan N, Senthil P, Vinodh S, Jayanth N (2017) A review on composite materials and process parameters optimisation for the fused deposition modelling process. *Virtual Phys Prototyp* 12:47–59. <https://doi.org/10.1080/17452759.2016.1274490>
13. Lalegani Dezaki M, MohdAriffin MKA, Hatami S (2021) An overview of fused deposition modelling (FDM): research, development and process optimisation. *Rapid Prototyp J* 27:562–582. <https://doi.org/10.1108/RPJ-08-2019-0230>

14. Bhoraskar A, Fartyal A, Sakthivel P (2017) Analysis of the Double Wishbone front suspension system. In: 2017 International Conference on Nascent Technologies in Engineering (ICNTE), Vashi, India. IEEE, pp 1–5. <https://doi.org/10.1109/ICNTE.2017.7947899>
15. Öhammar Anton, Grundén Jacob, Jaleby Jon, et al (2017) Design and 3D Printing of Down-scaled Passenger Vehicle Chassis. Chalmers University of Technology
16. Griesse D, Namouz E, Shankar P et al (2011) Application of a Lightweight Engineering Tool: Lazy Parts Analysis and Redesign of a Remote Controlled Car. In: Volume 8: 11th International Power Transmission and Gearing Conference; 13th International Conference on Advanced Vehicle and Tire Technologies. ASMEDE, pp 839–847. <https://doi.org/10.1115/DETC2011-47544>
17. Al-Asady NA, Abdullah S, Ariffin AK et al (2009) Comparison between experimental road data and finite element analysis data for the automotive lower suspension arm. *Eur J Sci Res* 29:557–571
18. Kannan S, Ramamoorthy M (2020) Mechanical characterization and experimental modal analysis of 3D Printed ABS, PC and PC-ABS materials. *Mater Res Express* 7:015341. <https://doi.org/10.1088/2053-1591/ab6a48>
19. Dunaj P, Berczyński S, Miądllicki K et al (2020) Increasing damping of thin-walled structures using additively manufactured vibration eliminators. *Materials* 13:2125. <https://doi.org/10.3390/ma13092125>
20. Parpala RC, Popescu D, Pupaza C (2021) Infill parameters influence over the natural frequencies of ABS specimens obtained by extrusion-based 3D printing. *Rapid Prototyp J* 27:1273–1285. <https://doi.org/10.1108/RPJ-05-2020-0110>
21. Rahman H, Yarali E, Zolfagharian A et al (2021) Energy absorption and mechanical performance of functionally graded soft-hard lattice structures. *Materials* 14:1366. <https://doi.org/10.3390/ma14061366>
22. Asadollahi-Yazdi E, Gardan J, Lafon P (2022) Generic roughness meta-model in 3D printing by fused deposition modeling. *Prog Addit Manuf* 7:399–410. <https://doi.org/10.1007/s40964-021-00237-8>
23. Yang L, Harrysson O, West H, Cormier D (2015) Mechanical properties of 3D re-entrant honeycomb auxetic structures realized via additive manufacturing. *Int J Solids Struct* 69–70:475–490. <https://doi.org/10.1016/j.ijsolstr.2015.05.005>
24. Noroozi R, Bodaghi M, Jafari H et al (2020) Shape-adaptive metastructures with variable bandgap regions by 4D printing. *Polymers (Basel)* 12:519. <https://doi.org/10.3390/polym12030519>
25. Saufi SASA, Zuhri MYM, Dezaki ML et al (2021) Compression behaviour of bio-inspired honeycomb reinforced starfish shape structures using 3D printing technology. *Polymers (Basel)* 13:4388. <https://doi.org/10.3390/polym13244388>
26. Yousefi A, Jolaiy S, Lalegani Dezaki M et al (2023) 3D-printed soft and hard meta-structures with supreme energy absorption and dissipation capacities in cyclic loading conditions. *Adv Eng Mater* 25:2201189. <https://doi.org/10.1002/adem.202201189>
27. Chen Y, Li T, Jia Z et al (2018) 3D printed hierarchical honeycombs with shape integrity under large compressive deformations. *Mater Des* 137:226–234. <https://doi.org/10.1016/j.matdes.2017.10.028>
28. Bhandari S, Lopez-Anido R (2019) Finite element modeling of 3D-printed part with cellular internal structure using homogenized properties. *Prog Addit Manuf* 4:143–154. <https://doi.org/10.1007/s40964-018-0070-2>
29. Ramazani H, Kami A (2022) Metal FDM, a new extrusion-based additive manufacturing technology for manufacturing of metallic parts: a review. *Prog Addit Manuf* 7:609–626. <https://doi.org/10.1007/s40964-021-00250-x>
30. Chadha U, Abrol A, Vora NP et al (2022) Performance evaluation of 3D printing technologies: a review, recent advances, current challenges, and future directions. *Prog Addit Manuf* 7:853–886. <https://doi.org/10.1007/s40964-021-00257-4>
31. Freitas D, Almeida HA, Bártoło H, Bártoło PJ (2016) Sustainability in extrusion-based additive manufacturing technologies. *Prog Addit Manuf* 1:65–78. <https://doi.org/10.1007/s40964-016-0007-6>
32. Lalegani Dezaki M, Ariffin MKAM, Appalanaidoo D et al (2022) 3D printed object's strength-to-weight ratio analysis for M3 liquid material. *Adv Mater Process Technol* 8:1610–1624. <https://doi.org/10.1080/2374068X.2020.1860596>
33. Loh GH, Pei E, Harrison D, Monzón MD (2018) An overview of functionally graded additive manufacturing. *Addit Manuf* 23:34–44. <https://doi.org/10.1016/j.addma.2018.06.023>
34. Cojocaru V, Frunzaverde D, Miclosina C-O, Marginean G (2022) The influence of the process parameters on the mechanical properties of PLA specimens produced by fused filament fabrication—a review. *Polymers (Basel)* 14:886. <https://doi.org/10.3390/polym14050886>
35. Dev S, Srivastava R (2021) Effect of infill parameters on material sustainability and mechanical properties in fused deposition modelling process: a case study. *Prog Addit Manuf* 6:631–642. <https://doi.org/10.1007/s40964-021-00184-4>
36. Mishra R, Powers WB, Kate K (2022) Comparative study of vibration signatures of FDM 3D printers. *Prog Addit Manuf.* <https://doi.org/10.1007/s40964-022-00323-5>
37. Georgiev Z, Kunchev L (2018) Study of the vibrational behaviour of the components of a car suspension. *MATEC Web Conf* 234:02005. <https://doi.org/10.1051/mateconf/201823402005>
38. Palmieri M, Zucca G, Moretini G et al (2022) Vibration fatigue of FDM 3D printed structures: the use of frequency domain approach. *Materials* 15:854. <https://doi.org/10.3390/ma15030854>
39. Messana A, Ferraris A, Airale AG et al (2020) Enhancing vibration reduction on lightweight lower control arm. *Shock Vib* 2020:1–15. <https://doi.org/10.1155/2020/8891831>
40. Davis JR (2004) Tensile Testing, Second edition. ASM International. pp 137–153. <https://doi.org/10.31399/asm.tb.tt2.t51060137>
41. Tohyama M (2011) Oscillation and resonance. Springer, Berlin, Heidelberg, pp 9–30. https://doi.org/10.1007/978-3-642-20122-6_2

Publisher's Note Springer Nature remains neutral with regard to jurisdictional claims in published maps and institutional affiliations.

Springer Nature or its licensor (e.g. a society or other partner) holds exclusive rights to this article under a publishing agreement with the author(s) or other rightsholder(s); author self-archiving of the accepted manuscript version of this article is solely governed by the terms of such publishing agreement and applicable law.